



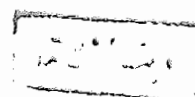
THE THEORY OF RESONANT TRANSFER EXCITATION IN ION-ATOM COLLISIONS

Thesis

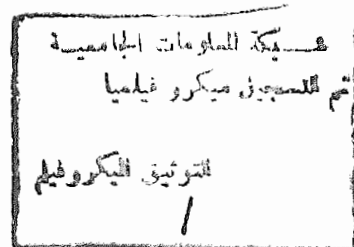
Submitted for the Degree of Doctor of Philosophy
in Physics

From the Faculty of Science

Ain Shams University



530.1
M.M



By

MAHMOUD MOHAMMAD YASEEN EL-BAKRY

49507

B.Sc., Physics, Ain Shams University

M.Sc., Physics, Ain Shams University

1994



TABLE OF CONTENTS

ACKNOWLEDGEMENTS	1
ABSTRACT	2
CHAPTER 1: INTRODUCTION	3
CHAPTER 2: ANALYSIS OF ION-ATOM COLLISIONS (Theoretical background)	8
2.1 Introduction	8
2.2 Similarity Between Resonant Transfer Excitation followed by X-rays (RTEX) and Dielectronic Recombination (DR) Processes	9
2.3 Auger Transition Process and Rate	10
2.3.1 Auger emission rates	11
2.3.2 Radiationless capture probability (V_a)	12
2.3.3 Continuum and bound state wave functions	13
2.3.3(a) Continuum wave function	13
2.3.3(b) Bound state wave function	15
2.4 Radiative Rates (A_r)	21
2.5 Atomic Parameters of Resonance States ($\Gamma(d)$, $\tau(d)$, $\omega(d)$)	23
2.6 DR Cross Sections	25
2.7 RTEX Cross Sections	28
2.8 The Compton Profile	33
2.9 DR Rate Coefficients (α^{-DR})	34



CHAPTER 3: RESONANT TRANSFER AND EXCITATION FOR $\text{Ca}^{16+}, 17+, 18+$ IONS	37
3.1 Introduction	37
3.2 Angular Momentum Average (AMA) Scheme	38
3.3 The results of DR, RTEX Cross Section for $\text{Ca}^{16+}, 17+, 18+$ Ions	42
3.3.1 Ca^{16+}	43
3.3.2 Ca^{17+}	50
3.3.3 Ca^{18+}	53
3.4 RTEX Trends for Ca Ions	56
3.5 Conclusions	59
CHAPTER 4: DR AND RTEX ISOELECTRONIC TRENDS OF C-LIKE IONS	60
4.1 Introduction	60
4.2 Method of Calculations	61
4.3 DR and RTEX Cross Sections for S^{10+} , Ca^{14+} and Fe^{20+}	64
4.3.1 S^{10+}	65
4.3.2 Ca^{14+}	73
4.3.3 Fe^{20+}	78
4.4 Isoelectronic Trends of DR, RTEX Cross Sections	
For C-like S^{10+} , Ca^{14+} and Fe^{20+} ions:	86
4.4.1 The Auger and Radiative Widths	86
4.4.2 Trends of DR Cross Sections	88
4.4.3 Trends of RTEX Cross Sections	92
4.5 Conclusions	94

CHAPTER 5: ISONUCLEAR TRENDS OF DR AND RTECH CROSS SECTIONS FOR Fe IONS	96
5.1 Introduction	96
5.2 Method of Calculations	97
5.3 Results and Discussions	98
5.3.1 DR, RTECH cross sections for Fe^{20+} , Fe^{18+} and Fe^{17+} with K-shell excitation	102
5.3.1a Fe^{20+}	104
5.3.1b Fe^{18+}	104
5.3.1c Fe^{17+}	109
5.3.2 DR, RTECH cross sections for $\text{Fe}^{20+, 18+, 17+}$ with L-shell excitation	114
5.3.3 Isonuclear trends of DR, RTECH cross sections for $\text{Fe}^{20+, 18+, 17+}$ ions	140
5.3.3a Trends of σ^{DR} with K- and L-shell Excitation	140
5.3.3b Trends of RTECH Cross Sections	141
5.3.4 DR rate coefficients for $\text{Fe}^{20+, 18+, 17+}$	146
5.4 Conclusions	152
SUMMARY	154
REFERENCES	157
ABSTRACT SUMMARY	

List of Tables

	page
Table (3-1) All d-states with 1s-excitation for $\text{Ca}^{16+,17+,18+}$ ions.	42
Table (3-2) DR cross section σ^{DR} for 1s-excitation of Ca^{16+} in units of 10^{-21} cm^2 with energy bin size $\Delta e_c = 1.0 R_y$. All data here are in AMA scheme.	45
Table (3-3) DR cross section σ^{DR} in units of 10^{-21} for Ca^{17+} with 1s-excitation with and without cascade corrections.	51
Table (3-4) The K-shell DR cross section for Ca^{18+} in units of 10^{-21} cm^2 with and without cascade effect.	54
Table (3-5) The values of the two peaks of RTECH cross sections in units of 10^{-21} cm^2 for $\text{Ca}^{16+,17+,18+}$ ions in AMA schemes.	56
Table (4-1) The Auger widths $\bar{\Gamma}_a(d)$ and radiative widths $\bar{\Gamma}_r(d)$ in sec^{-1} in AMA scheme for dominant states of S^{10+} with K-shell excitation.	66
Table (4-2) DR cross section σ^{DR} in units of 10^{-21} cm^2 for S^{10+} with 1S-excitation with and without cascade corrections.	67
Table (4-3) DR cross section σ^{DR} with and without cascade correction in units of 10^{-21} cm^2 for Ca^{14+} with K-shell excitation.	74
Table (4-4) DR cross section for Fe^{20+} with and without cascade effect.	79
Table (4-5) Resonance widths $\bar{\Gamma}_a(d)$, $\bar{\Gamma}_r(d)$ and $\bar{\Gamma}(d)$ (in sec^{-1}) for the dominant intermediate states formed in the collision of S^{10+} , Ca^{14+} and Fe^{20+} with continuum electrons. K-shell excitation is assumed.	87

Table (4-6)	Cascade DR cross section in units of 10^{-21} cm^2 for C-like (S^{10+} , Ca^{14+} and Fe^{20+}) with 1S-excitation.	89
Table (5-1)	All states with 1s-excitation for $\text{Fe}^{20+, 18+, 17+}$ ions.	103
Table (5-2)	The DR cross sections for Fe^{18+} with 1s-excitation in units of 10^{-21} .	106
Table (5-3)	DR cross section σ^{DR} in units of 10^{-21} cm^2 for Fe^{17+} with 1s-excitation before and after cascade corrections.	110
Table (5-4)	DR cross section σ^{DR} in units of 10^{-21} cm^2 before and after cascade correction for Fe^{20+} with 2s-excitation.	115
Table (5-5)	DR cross section σ^{DR} in units of 10^{-21} cm^2 with and without cascade for Fe^{20+} with 2p-excitation.	118
Table (5-6)	DR cross section σ^{DR} in units of 10^{-21} cm^2 with and without cascade for Fe^{18+} with 2s-excitation.	125
Table (5-7)	DR cross section σ^{DR} in units of 10^{-21} cm^2 with 2p-excitation for Fe^{18+} .	127
Table (5-8)	σ^{DR} with and without cascade effect for Fe^{17+} with 2s-excitation in units (10^{-21} cm^2).	133
Table (5-9)	σ^{DR} vs $e_c(R_y)$ for Fe^{17+} with 2p-excitation in units of 10^{-21} cm^2 .	136
Table (5-10)	Total DR cross sections for iron ions ($\text{Fe}^{20+, 18+, 17+}$) with K- and L- shell excitation.	140
Table (5-11)	The maximum dielectronic recombination rate coefficient ($\alpha^{\text{DR}}_{\text{max}}$) for $\text{Fe}^{20+, 18+, 17+}$ with 1s, 2s and 2p-excitations.	147

List of Figures

	page	
Fig. (3-1)	The RTEX cross sections for the system $\text{Ca}^{16+} + \text{H}_2$ with 1s-excitation versus the ionic projectile energy.	49
Fig. (3-2)	As in Fig. (3-1), but for the collisional system $\text{Ca}^{17+} + \text{H}_2$.	52
Fig. (3-3)	As in Fig. (3-1), but for the collisional system $\text{Ca}^{18+} + \text{H}_2$.	55
Fig. (3-4)	RTEX cross sections (10^{-21} cm^2) for the systems $\text{Ca}^{z+} + \text{H}_2$, ($z=16,17,18$) with 1s-excitation versus the ion beam energy.	58
Fig. (4-1)	σ^{DR} for S^{10+} with 1s-excitation versus the continuum energy.	68
Fig. (4-2)	Same as Fig. (4-1), but at energy bin size = 10 Ry	70
Fig. (4-3)	σ^{RTEX} for $\text{S}^{10+} + \text{H}_2$ collisional system with 1s-excitation versus the projectile energy.	71
Fig. (4-4)	Same as fig. (4-3) but, for the He target.	72
Fig. (4-5)	σ^{RTEX} with 1s-excitation for the system $\text{Ca}^{14+} + \text{H}_2$ in units of 10^{-21} cm^2 versus Ei (Mev.).	76
Fig. (4-6)	Same as fig. (4-5) but, for $\text{Ca}^{14+} + \text{H}_0$ process.	77
Fig. (4-7)	Cascade corrected DR cross section σ^{DR} (10^{-22} cm^2) for Fe^{20+} with K-shell excitation versus the energy of incident electron.	82
Fig. (4-8)	K-shell RTEX cross section for the system $\text{Fe}^{20+} + \text{H}_2$ versus ion beam energy Ei.	84
Fig. (4-9)	As in fig. (4-8) but, for the $\text{Fe}^{20+} + \text{H}_0$ collisional system.	85
Fig. (4-10)	The isoelectronic trends of σ^{DR} for C-like S^{10} , Ca^{14+} and Fe^{20+} versus the continuum energy.	91

Fig. (4-11)	Trends of σ^{RTEX} for the collision of C-like S^{10} , Ca^{14+} and Fe^{20+} with the H_2 target. The K-shell excitation is assumed in the calculations.	93
Fig. (5-1)	K-shell RTEX cross section for the system $\text{Fe}^{18+}+\text{H}_2$ versus ion beam energy E_i .	107
Fig. (5-2)	Same as in fig. (5-1) but, for the system $\text{Fe}^{18+}+\text{H}_e$.	108
Fig. (5-3)	RTEX cross section for the $\text{Fe}^{17+}+\text{H}_2$ with K-shell excitation.	112
Fig. (5-4)	RTEX cross sections for $\text{Fe}^{17+}+\text{H}_e$ with 1s-excitation.	113
Fig. (5-5)	The DR cross section for Fe^{20+} with L-shell excitation versus the incident electron energy.	121
Fig. (5-6)	L-shell RTEX cross sections for the system $\text{Fe}^{20+}+\text{H}_2$ versus the ion beam energy E_i	122
Fig. (5-7)	L-shell RTEX cross sections for the system $\text{Fe}^{20+}+\text{H}_e$ versus the ion beam energy E_i .	123
Fig. (5-8)	DR cross section σ^{DR} for Fe^{18+} with L-shell excitation.	129
Fig. (5-9)	RTEX cross sections σ^{RTEX} for the system $\text{Fe}^{18+}+\text{H}_2$ with L-shell excitation versus the ion beam energy E_i	131
Fig. (5-10)	σ^{DR} versus e_c (Ry) for Fe^{17+} with L-shell excitation in units of 10^{-20} cm^2	138
Fig. (5-11)	σ^{RTEX} in units of 10^{-21} cm^2 versus ion beam energy E_i for the system $\text{Fe}^{17+}+\text{H}_2$. L-shell excitation is considered.	139
Fig. (5-12)	Isonuclear trends of the RTEX cross sections for the collision of Fe ions with H_2 . K-shell excitation is considered.	142
Fig. (5-13)	Same as fig. (5-12) but, L-shell excitation is assumed.	145

Fig. (5-14)	Dielectronic recombination rate coefficients for Fe^{20+} with 1S-, 2S- and 2P-excitations versus the temperature, KT, of the incident electron (in kev.).	148
Fig. (5-15)	Same as fig. (5-14), but for Fe^{18+} .	149
Fig. (5-16)	Same as fig. (5-15), but for Fe^{17+} .	150
Fig. (5-17)	The variation of α^{DR} with the electron temperature KT in kev. for the Fe^{20+} , $18+$, $17+$ ions with 1S, 2S and 2P-excitations.	151

ACKNOWLEDGMENTS

I would like to express my deep gratitude to Prof. Dr. Ali Helmy Moussa, Professor of Theoretical Physics, for suggesting the problems in this thesis, for his continuous guidance, and his support.

I am very grateful to Dr. Gaber Omar, Assistant Professor of Theoretical Physics, for his continuous supervision and his sincere guidance through the whole period of preparation of this thesis.

Special thanks are due to Dr. Atef Khazbak, Lecturer of Theoretical physics for his great help.

I would like to thank Prof. Dr. Karimat El-Sayed, The Head of the Department for her valuable encouragement.

My deep thanks are due to Prof. Dr. A.A. El-Shazly, previous head of Department of Physics, Faculty of Education, Ain Shams University for his great help during the period of preparation of the thesis.

Most of the calculations done in this thesis were carried out in the IBM Scientific Center, Cairo, the big help offered by the staff there is greatly acknowledged. Also the help offered by the staff of Ain Shams University Computing Center is highly appreciated.

My sincere thanks are due to the Theoretical Physics Group, especially Dr. Hassan Hassan Ramadan.

Special thanks should be expressed to my family, who suffered so much from my absence the last four years.

ABSTRACT

RTEX cross sections are calculated for the collision of $\text{Ca}^{16+, 17+, 18+}$ ions with He and H_2 with K-shell excitation and found in agreement with experimental and theoretical data (Badnell 1990). In addition, RTEX cross sections are carried out for C-like S^{10+} , Ca^{14+} , Fe^{20+} with K-shell excitation. The isoelectronic trends of RTEX for C-like ions are discussed. Finally, the RTEX cross sections are calculated for $\text{Fe}^{20+, 18+, 17+}$ with both K- and L-shell excitations. The isonuclear trends of RTEX for Fe-isonuclear sequence are discussed and explained. RTEX cross sections for L-shell excitation are huge relative to the K-shell excitations. Thus, RTEX process manifests itself as a more efficient mechanism for outer shell excitation.

CHAPTER 1

INTRODUCTION

CHAPTER I

INTRODUCTION

In astrophysical and laboratory plasmas, various atomic processes are taking place, for example: electron-electron, electron-ion, and ion-atom collisions.

The resonant transfer excitation followed by X-rays (RTEX) in ion-atom (I/A) collisions is a process of much interest in the current research, experimentally and theoretically, since the last decade. It proceeds through the formation of doubly-excited resonance intermediate states which may be stabilized also by emission of Auger electrons (RTEA). Thus, RTEX and RTEA are two complementary processes in I/A collisions.

The RTEX process that occurs in I-A collisions, is a similar process to the dielectronic recombination (DR) in electron-ion (e-I) collisions. When the conditions of the impulse approximation are satisfied for I/A collisions, the RTEX and DR cross sections are related. Hence, RTEX cross sections are considered as indirect measurements for the DR cross sections. In addition, RTEX is successful in the explanation of the theoretical DR cross sections especially those with small values for $\Delta n \neq 0$ transitions, where Δn is the change in the principal quantum number n . Moreover, RTEX is still the main source of experimental data for DR in highly charged ions.

The DR process is an important recombination mechanism that affects the ionization balance of plasmas and is of interest in plasma diagnostics. The emission of X-rays in both RTEX and DR causes the self-cooling of plasmas which make them of special interest in theoretical and experimental studies each in its own right and through their relationship.

The relationship between DR and RTEX processes has been formulated by Brandt (1983) and verified theoretically by MacLaughlin and Hahn (1984, 1985), Omar and Hahn (1987), Hahn et al (1987), Hahn and LaGattuta (1988), Badnell (1990, 1993) and Omar (1992). This was in parallel to the experimental work by Tanis et al (1982, 1984, 1985, 1986), Bernstein et al (1986, 1987, 1989), Reusch et al (1988), Graham et al (1986) Schonfeldt et al (1987) for measuring the RTEX cross sections. Also, very recent experiments were carried out for measuring the DR cross sections by Dewitt et al (1991, 1992, 1993) and Knapp et al (1993) which invoked the theoretical work on heavy ions.

The intensive and extensive experimental and theoretical works on RTEX and DR processes in parallel to the other atomic processes such as ionization and excitation are still continuing to improve the knowledge and understanding of the factors affecting the time rate of change of the number of ions in a plasma. This, when completed, will bring the plasma energy to the field of reality.

Unfortunately, there is a gap in the available theoretical data for B-like up to F-like ions in RTEX and DR cross sections.